

Proton NMR Determination of Miscibility in a Bulk Model Photoresist System: Poly(4-hydroxystyrene) and the Photoacid Generator, Di(*tert*-butylphenyl)Iodonium Perfluorooctanesulfonate

D. L. VanderHart,* V. M. Prabhu, and E. K. Lin

Polymers Division, National Institute of Standards and Technology,
Gaithersburg, Maryland 20899

Received December 1, 2003. Revised Manuscript Received May 13, 2004

The intimacy of component mixing in solvent-cast blends of poly(4-hydroxystyrene) (PHS) and a photoacid generator (PAG), di(*tert*-butylphenyl)iodonium perfluorooctanesulfonate (PFOS) were studied by solid-state proton NMR. These are simplified blends for chemically amplified photoresist formulations used in the micro-electronics industry. Multiple-pulse NMR techniques are used in both spin-diffusion and longitudinal relaxation experiments at ambient temperatures. It is deduced that PFOS is mixed with PHS on a molecular scale for the mass-ratio range investigated, namely, 91/9 to 55/45 PHS/PFOS; hence, the two components are thermodynamically miscible in this range. Control experiments involving a 91/9 physical mixture of PHS and PFOS as well as solvent-cast blends of polystyrene (PS) and PFOS serve to illustrate the contrast between data obtained for phase-separated blends and data for blends that display molecular level mixing. An attempt was also made to support the notion of intimate PFOS/PHS mixing by looking for evidence of ^1H – ^{19}F dipolar broadening in multiple-pulse blend spectra. This attempt was not successful owing to rapid polarization exchange between ^{19}F nuclei. These results, extendable to next-generation resist formulations, should also prove useful for characterizing photoacid/resist dispersions for sub-100 nm critical dimension control.

Introduction

Photoresists are the key patterning materials used for the fabrication of integrated circuits. Photoresist formulations are highly tuned, multicomponent mixtures consisting primarily of a polymer matrix, photoacid generator (PAG), base additives, and usually dissolution inhibitors. After a thin film is applied to a solid support via spin coating, the sample is post-apply baked (PAB) below the nominal glass transition temperature to remove residual solvent. It is then exposed to UV radiation through a patterned mask to photo-generate the acidic species that catalyzes the deprotection chemistry during the post-exposure bake (PEB). It is the diffusion of the acid within the UV exposed regions during the PEB that leads to the image that is finally developed using an aqueous base developer.^{1,2}

Many current 248-nm chemically amplified photoresist formulations use a copolymer of poly(4-*tert*-butoxycarbonyloxystyrene) (PBOCSt) with poly(4-hydroxystyrene) (PHS). PBOCSt moieties are deprotected to form more PHS via the action of the acid catalytic PAG during the PEB. In a typical formulation, the copolymer mass ratio is 80/20 PHS/PBOCSt. It is critical to the function of the photoresist that the PAG and the

polymer are initially mixed on a level much more intimate than the critical dimensions in the final pattern. To ensure that the initial distribution of the PAG in the polymer is not responsible for creating undesirable line edge roughness, one would like to ascertain its thermodynamic compatibility with the polymer. Knowledge of the quality of PAG dispersion (along with some knowledge of quantum efficiency and number of catalyzed reactions per PAG molecule³) will also help in computer modeling the deprotection process. Presumably, if a significant fraction of PAG aggregates within a thin film, then the photoacid diffusivity during PEB would be more heterogeneous and complicated relative to that of a uniformly dispersed PAG.

In this paper, we demonstrate, using solid-state proton NMR techniques, the mixing of a particular PAG, di(*tert*-butylphenyl)iodonium perfluorooctanesulfonate (PFOS), into the model polymer (PHS) in acetone-precipitated, bulk samples of PHS/PFOS blends ranging in mass ratio from 91/9 to 55/45. Obviously this is not the reactive copolymer, but it is closely related by stoichiometry and chemistry. Also, these are bulk samples, as opposed to thin films and the solvent (acetone) is much more volatile than the solvents used in photoresist film casting. However, in view of the intimate mixing of the components observed in this study, expectations that PFOS would be well-mixed in

* Corresponding author phone: (301)975-6754; fax: (301)975-3928; e-mail: david.vanderhart@nist.gov.

(1) Wallraff, G. M.; Hinsberg, W. D. *Chem. Rev.* **1999**, *99*, 1801–1821.

(2) Ito, H. *IBM J. Res. Dev.* **2000**, *44*, 119–130.

(3) McKean, D. R.; Schaedeli, U.; MacDonald, S. A. *J. Polym. Sci. A Polym. Chem.* **1989**, *27*, 3927–3935.

the PHS/PBOCSt copolymer thin films are certainly raised.

Experimental Section

Samples. The PHS has $M_{w,r}$ of 5260 g/mol and $M_{n,r}$ of 4686 g/mol. A 4% (by mass) solution was made by codissolving PHS and PFOS in the intended mass ratios (91/9, 85/15, 70/30, 55/45) in 2.8 g of acetone. The solution was filtered using a 0.2-mm poly(tetrafluoroethylene) filter and then poured into a glass watch glass. After the acetone evaporated, the sample was baked in an oven at 100 °C for 180 s leaving a dry sample that was subsequently scraped off with a ceramic spatula. The dried white powder was transferred to a glass vial and vacuum-dried overnight at 45 °C. About 20 mg of dried solid was then quickly transferred under red light into a 4 mm i.d./4 mm high cylindrical cavity in a 5 mm o.d. NMR rotor made of zirconia.

Blends, 96/4 and 91/9, of polystyrene (PS) and PFOS were made in a similar way using tetrahydrofuran (THF) as the solvent. The PS had $M_{n,r}$ of 24 000 g/mol and $M_{w,r}$ of 24 700. Materials were cast into a poly(tetrafluoroethylene) dish. After evaporation of the solvent and oven drying overnight at 45 °C, the remaining solids were scraped from the dish, and a portion of each sample was analyzed. Given that we expected phase separation of these PS and PFOS components, the preparation method leaves open the possibility that the stoichiometry of the analyzed sample is not exactly that of the original mixture.

A 91/9 physical mixture of PHS and PFOS was made by weighing the pure materials, combining them as solids, and placing the entire mass of materials into the rotor.

NMR. The 300 MHz proton multiple-pulse (MP) spectra were taken at ambient temperature (20 °C) using a 7.05 T Bruker⁴ Avance spectrometer (Bruker Biospin Corporation, Billerica, MA) equipped with a low-proton-background probe (Doty Scientific, Inc., Columbia, SC). Magic-angle-spinning (MAS)^{5,6} and multiple-pulse (MP)⁷⁻⁹ techniques were both employed, yielding so-called CRAMPS¹⁰ spectra (Combined Rotation and Multiple Pulse Spectroscopy) in which (a) the proton-proton dipolar interaction is suppressed by MP and (b) MAS averages away chemical shift anisotropy along with isotropic magnetic susceptibility effects. CRAMPS spectra are solid-state analogues of high-resolution proton spectra. Achievable resolution is generally only modest, and line widths are typically on the order of 2 ppm in noncrystalline solids.

Pulse sequences include a "chemical-shift-based" spin-diffusion sequence¹¹⁻¹³ and an inversion-recovery¹⁴ sequence with CRAMPS readout. In the former experiment, we initially create a desired magnetization gradient using 20 cycles of an MREV-8-style^{8,9} CRAMPS pulse sequence. We chose a MAS frequency of 2525 Hz so that this 20-cycle preparation would take exactly two rotor periods. At the end of this period, magnetization is stored, on alternate scans, as positive or negative Zeeman polarization. This preparation produces

magnetization whose initial profile is that of a CRAMPS spectrum that has been multiplied by a sinusoidal function whose origin (dictated by frequency offset) and period (8.4 ppm in this case, as dictated by the number of cycles) are under experimental control. Then, following a variable spin-diffusion (SD) time (t_{sd}) the polarization is read out as a CRAMPS spectrum. These so-called SD spectra, as a function of t_{sd} , move from their sinusoidally modulated initial condition toward internal spin equilibration. Sample-wide internal spin equilibrium is evidenced by a return to the M_0 CRAMPS line shape; however, this is a nonequilibrium experiment in the sense that, at long times, all polarizations will also move toward their Boltzmann values. Thus, in this SD experiment, one tries to achieve spin equilibration in a short time as compared with the longitudinal relaxation time (T_1^H). We met this criterion in the current work by limiting our SD experiment, for the cases of well-mixed blends, to $t_{sd} < 0.08 T_1^H$. Proton radio frequency fields corresponded to a 167 kHz nutation frequency (1.5 μ s 90° pulse), and the MREV-8 cycle time was 39.6 μ s.

Small background signals, particularly from the rotor endcaps and spacers, can interfere with the interpretation of these SD spectra; hence, we duplicate each experiment using a rotor that contained only the endcaps and spacers in their normal positions. On the basis of these spectra, we adjusted our SD spectra to compensate for these small, extraneous signals. The probe is a low-proton-background probe, but in the present case where, for the 91/9 PHS/PFOS blend, the expected stoichiometric fraction of PFOS protons is only 4.1% of the total, it is necessary to make these background corrections. For example, these corrections were approximately 10% and 4% of the total intensity for the 91/9 and 85/15 blend data, respectively.

SD data are plotted against the square root of the SD time, t_{sd} . The ordinate, $\Delta M(t_{sd})$, in these plots has been defined in detail in a previous paper¹⁵ and is given by the formula

$$\Delta M(t_{sd}) = \exp(t_{sd}/T_1^H) [P_{\text{PFOS}}(t_{sd}) - (I(t_{sd})/I_{M_0}) / [P_{\text{PFOS}}(t_{sd} = 0) - P_{\text{BLEND}}(t_{sd} = 0)] \quad (1)$$

where $I(t_{sd})$ and I_{M_0} are respectively the total integrals of the SD spectrum at t_{sd} and of the M_0 spectrum of the blend. Thus, $I(t_{sd})/I_{M_0}$ is the sample-average polarization at t_{sd} . (Actually, this is a relative polarization where the Boltzmann polarization is taken to be 1.00.) The term $\exp(t_{sd}/T_1^H)$ compensates for amplitude loss attributed to T_1^H , where the latter quantity is independently measured. $P_{\text{PFOS}}(t_{sd})$ and $P_{\text{PFOS}}(t_{sd} = 0)$ are, respectively, polarization levels of PFOS protons at t_{sd} and $t_{sd} = 0$ whereas $P_{\text{BLEND}}(t_{sd} = 0)$ is the initial average polarization level for all the protons in the blend. The latter can be determined by extrapolating the ratio $I(t_{sd})/I_{M_0}$ to $t_{sd} = 0$. Thus, $\Delta M(t_{sd})$ is a scaled quantity that tracks the relative changes in average PFOS polarization between its initial value ($\Delta M(t_{sd}) = 1.00$) and its value if and when sample-wide spin equilibrium ($\Delta M(t_{sd}) = 0.0$) is achieved. If domains in a phase-separated blend are very large and unmixed, then $\Delta M(t_{sd})$ should remain at 1.00 throughout the SD experiment. Embodied in eq 1 is the notion that, for a given two-component system, polarization changes caused by intermolecular SD only depend on the initial polarization gradient between the components and not on the polarizations themselves. Hence, a quantity like $\Delta M(t_{sd})$, that is scaled by this initial gradient, will capture the appropriate time dependence of the SD process for all applied gradients. The quantity $\Delta M(t_{sd})$ strictly refers to a magnetization, not a polarization, with the former being the product of polarization times the number of spins. We keep this nomenclature in order to be consistent with literature notation¹⁵ recognizing that polarization and magnetization are proportional and that we are dealing with relative quantities. On the other hand, it is important to appreciate the following distinction, namely, that during SD the total magnetization remains the same in the absence of T_1^H effects, even though

(4) Certain commercial companies are named in order to specify adequately the experimental procedure. This in no way implies endorsement or recommendation by NIST.

(5) Andrew, E. R. *Prog. Nucl. Magn. Reson. Spectrosc.* **1972**, *8*, 1.

(6) Lowe, I. J. *Phys. Rev. Lett.* **1959**, *2*, 85.

(7) Waugh, J. S.; Huber, L. M.; Haeberlen, U. *Phys. Rev. Lett.* **1968**, *20*, 180.

(8) Rhim, W.-K.; Elleman, D. D.; Vaughan, R. W. *J. Chem. Phys.* **1973**, *59*, 3740.

(9) Mansfield, P.; Orchard, J.; Stalker, D. C.; Richards, K. H. B. *Phys. Rev.* **1973**, *B7*, 90.

(10) Ryan, L. M.; Taylor, R. E.; Paff, A. J.; Gerstein, B. C. *J. Chem. Phys.* **1980**, *72*, 508.

(11) Caravatti, P.; Neuenschwander, P.; Ernst, R. R. *Macromolecules* **1985**, *18*, 119.

(12) Caravatti, P.; Neuenschwander, P.; Ernst, R. R. *Macromolecules* **1986**, *19*, 1895.

(13) Campbell, G. C.; VanderHart, D. L. *J. Magn. Res.* **1992**, *96*, 69.

(14) Farrar, T. C.; Becker, E. D. *Pulse and Fourier Transform NMR*; Academic Press: New York, 1971; pp 20-21.

(15) VanderHart, D. L.; McFadden, G. B. *Solid State Nucl. Magn. Reson.* **1996**, *7*, 45-66.

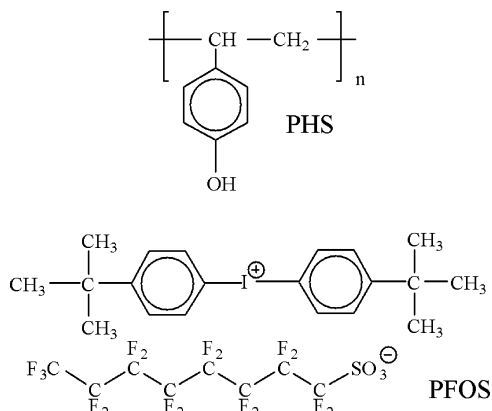


Figure 1. Chemical structures associated with PHS and PFOS.

by necessity the polarization changes are larger for the component with fewer protons.

In such plots, phase separation in a two-component system is indicated by a linear change in $\Delta M(t_{sd})$ at early times where the slope is proportional to the interface area separating the two components.¹⁵ Note that the denominator in eq 1 is the scaling constant. To obtain a properly scaled $\Delta M(t_{sd})$, one needs to know $P_{PFOS}(t_{sd} = 0)$ as well as the precise blend stoichiometry. To the degree that these quantities are uncertain, $\Delta M(t_{sd})$ will be improperly scaled; however, since uncertainties originating from improper scaling are proportional to $\Delta M(t_{sd})$, the error contribution from improper scaling approaches 0 as $\Delta M(t_{sd})$ approaches 0. Hence, scaling uncertainty creates no ambiguity in defining when spin equilibrium has been reached. In some of the cases discussed in this paper, there is uncertainty in scaling. A knowledge of $P_{PFOS}(t_{sd} = 0)$ is quite reliably obtained by separately measuring this polarization as a function of frequency offset for pure PFOS under experimental conditions identical to those applied to the blend. Because small variations in spectrometer tuning can cause spectral frequency shifts, PFOS shifts were always matched with those of the polarization–calibration spectra in order to establish the initial PFOS polarizations for the SD spectra of the blends. The larger uncertainty, in the cases discussed herein, arises because of uncertainties in the actual stoichiometry. We cannot easily use the equilibrium spectrum to verify composition since component line shapes are known with insufficient precision. It is easier to separate and integrate components using SD spectra in which PFOS line shape contributions have intensities of opposite sign to those of the other component. It is essential that the component intensities be quantified in the SD spectra. That is the principal reason that motivates the establishment of experimental parameters that yield SD spectra that have very small total integrals and a very good chance of component contributions of opposite sign. In eq 1, $P_{PFOS}(t_{sd})$, which is defined by the integral ratio $I_{PFOS}(t_{sd})/I_{PFOS}(M_0)$, is the quantity with the greatest uncertainty, primarily due to the uncertainty in $I_{PFOS}(M_0)$. The latter is effectively a second scaling constant in eq 1. If the stoichiometry were precisely known, $I_{PFOS}(M_0)$ could be calculated as the predicted fraction of the total M_0 intensity. If samples are thermodynamically compatible, as is found for all of the acetone-cast PHS/PFOS blends, it is much less likely that a portion of a prepared sample, used in the NMR experiment, has a stoichiometry that deviates from that of the original ingredients.

Results

The structures of PHS and PFOS are given in Figure 1. The PS structure is not shown, being related to that of PHS by the replacement of the hydroxy group with a proton. PHS and PS are atactic and do not crystallize. PFOS, by itself, is a crystalline ionic material comprised of a protonated cationic part and a perfluorinated

anionic part. The two principal strategies we employed for looking at the intimacy of mixing of PHS (or PS) and PFOS were the following: (a) measurement of the rate at which the PAG and PHS (PS) protons equilibrate via SD after an initial polarization gradient between the different protons is imposed and (b) detection of proton–¹⁹F dipolar interactions that would indicate proximity (up to about 0.5 nm) for the PHS (PS) protons and the PFOS ¹⁹F nuclei. Most of the discussion will deal with approach *a* since approach *b* was not successful. We will also include the probable reasons for failure of the latter approach.

It is noteworthy that attempts to measure the intimacy of mixing by neutron scattering methods¹⁶ in this PHS/PFOS system using partially deuterated PHS gave ambiguous results. While there might be some other combinations of protonated and deuterated species that would yield more information by neutron scattering, a clear advantage of this solid-state NMR approach is that no isotopic substitutions are necessary, nor is any chemical modification required.

Figure 2 shows the 300 MHz, 2.5 kHz MAS, CRAMPS spectra of the 91/9 PHS/PFOS blend, pure PHS, and pure crystalline PFOS. The PFOS spectrum is shown in Figure 2C and D with two vertical scalings. According to the stoichiometry, Figure 2B and D represent the expected ratio (95.9/4.1) of proton intensity contributions to the 91/9 blend spectrum. There is strong spectral overlap for all of these materials, and each has an aliphatic upfield and a principally aromatic downfield line. In the PHS spectrum, the hydroxy proton and the four aromatic protons of the monomer contribute to the downfield line, and the three aliphatic protons make up the upfield line. The 18 aliphatic protons of the PFOS molecule are found in the upfield region while the eight aromatic protons are downfield. Particularly note that the aliphatic lines of PFOS and PHS are characterized by different line widths (about 2.5 ppm for PHS and 1.2 ppm for PFOS). We will make use of this feature in the separation of PFOS and PHS signals in subsequent SD experiments. The slight splittings of the two groups of resonances in the spectrum of PFOS probably indicates magnetic inequivalence within the unit cell of crystalline PFOS. If PFOS is mixed into the blend, the environment of the PFOS molecules will vary more widely; hence, the PFOS resonances will broaden somewhat but will likely remain significantly narrower than those of the PHS. The blend spectrum resembles the PHS spectrum, except for the slightly stronger aliphatic resonance.

To conduct a SD experiment, we must produce an average polarization gradient between PHS and PFOS protons. We use the fact that the intensity ratios of the upfield and downfield lines are different for PHS and PFOS. Thus, we can perform a nonequilibrium, chemical-shift-based SD experiment and expect to produce, thereby, an average polarization gradient between the PHS and the PFOS protons.

The following are expected SD characteristics in two extreme limits. If the PHS and PFOS are intimately mixed, the spin equilibration time is short and of the order of a few milliseconds;¹⁷ if these components are

(16) Private communication from R. L. Jones and C. Soles of our laboratory.

(17) VanderHart, D. L. *Macromolecules* **1994**, *27*, 2837.

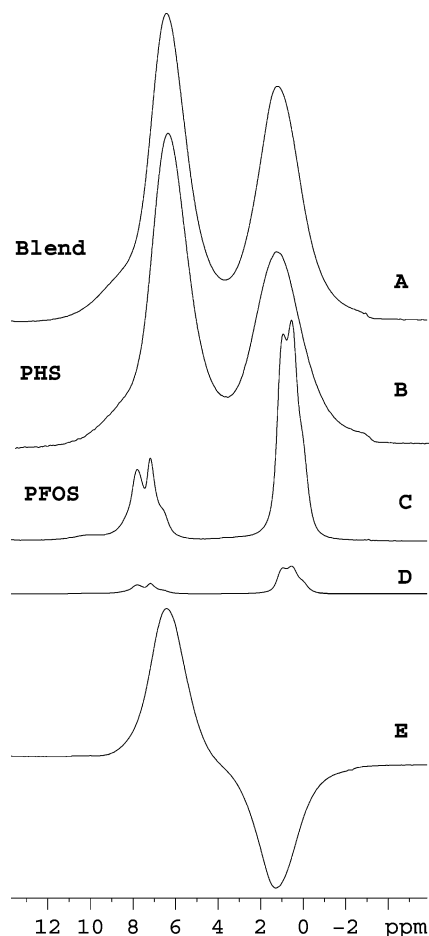


Figure 2. MREV-8 spectra at 300 MHz (2525 Hz MAS): acetone-cast 91/9 PHS/PFOS blend (A), pure PHS (B), pure PFOS (C and D, where the intensities of B and D are scaled in proportion to their expected proton ratio for a 91/9 blend). The spectrum (E) is associated with the chemical-shift-based spin-diffusion experiment ($t_{sd} = 20 \mu s$). This is the profile of the initial magnetizations generated by the preparation and is vertically scaled to provide a direct comparison with spectrum A. The total integral in E is intentionally close to zero. Spectra shown in Figure 3 are those taken at longer t_{sd} values.

phase-separated on a scale, say, larger than 200 nm, then there is little polarization exchange between PHS and PFOS protons.

In Figures 2E and 3, SD spectra for the 91/9 blend are shown as a function of t_{sd} . Initially ($t_{sd} = 20 \mu s$ in Figure 2E), the aromatic polarization is largely positive and the aliphatic polarization is largely negative. One can also get an indication of the initial aromatic and aliphatic polarization levels since Figure 2A and E are scaled to the same number of scans. Since SD proceeds by spin exchange events between dipolar coupled spin pairs,¹⁸ total magnetization, which is proportional to the total signal integral, is conserved in the absence of T_1^H effects. Moreover, since the total intensity in Figure 2E is chosen to be close to zero, the main line shape changes produced by polarization exchange between aliphatic and aromatic protons will be reductions in absolute intensity for both aromatic and aliphatic lines. Average polarization gradients also exist initially between PHS

protons and PFOS protons because of their different ratios of aliphatic and aromatic protons. However, even larger initial aromatic/aliphatic gradients exist within each component; thus changes in the spectra over the first 1 ms of t_{sd} are dominated by intramolecular polarization exchange, even though, as we shall see, there is also substantial intermolecular exchange during the same period. Note that at $t_{sd} = 1$ ms, the SD spectrum (Figure 3A) looks like the sum of a positive, broader aromatic line and a narrower, negative, aliphatic line. The broader resonance is typical of the PHS aromatics (Figure 2B) while the narrower line has a line width of 1.4 ppm, which is much closer to the 1.2 ppm PFOS line width (Figure 2C) than to the 2.5 ppm PHS line width. Thus, we attribute the negative-going aliphatic line mainly to the PFOS component. At the same time, we note that the mild splitting of the aliphatic resonance, seen in crystalline PFOS, is absent. This reduction in resolution is a qualitative indication that the PFOS is more dispersed in the blend.

At $t_{sd} = 2$ ms (spectrum 3B), the distinction between the PHS and the PFOS aliphatic line widths is clearer with the PFOS contribution remaining slightly negative. However, by $t_{sd} = 4$ ms, the aliphatic resonance seems quite broad, the negative PFOS contribution is no longer obvious, and the line shape changes are small (spectra 3D–H) through the longest t_{sd} value of 50 ms (Figure 3H). The latter spectrum is shown with a scaled-down (by $\times 0.0072$) version of the equilibrium (M_0) CRAMPS spectrum. This comparison shows that the 50-ms SD spectrum is very close to the M_0 line shape (i.e., sample-wide spin equilibration is nearly achieved). In Figure 3, we have also included “zero-integral” difference spectra (Figure 3I–P) generated by subtracting from each SD spectrum a scaled-down version of the M_0 spectrum, whose total integral is the same as that of the SD spectrum. Since the spectral changes driven by SD are only sensitive to polarization differences and since all components have the same polarization in the M_0 spectrum, these zero-integral spectra faithfully maintain the polarization differences embodied in each SD spectrum. After intramolecular spin equilibration is complete, zero-integral difference spectra will represent the positive (PHS) and negative (PFOS) polarizations as they approach “zero” (sample-wide spin equilibrium). One can see that for $t_{sd} > 10$ ms, very little change in PHS/PFOS polarization occurs.

Similar SD spectra for the 85/15, 70/30, and 55/45 blends were obtained. Some spectra pertaining to the 55/45 PHS/PFOS blend are shown in Figure 4, where the M_0 spectrum is compared with the zero-integral difference spectra obtained from the SD spectra. In this case (where the theoretical fraction of proton intensity belonging to PFOS is 0.26, instead of, say, 0.041 for the 91/9 blend), we have a better sensitivity for detecting any phase separation. As is clear from Figure 4, sample-wide spin equilibrium is closely approached after 10 ms of spin-diffusion. This was true for all of the acetone-cast blends of PHS and PFOS.

To show contrasting behavior for phase separated systems, Figures 5 and 6 illustrate the lack of spin-diffusion coupling, respectively, for a physically mixed 91/9 PHS/PFOS sample and for a 91/9 PS/PFOS sample cast from a THF solution. For the physical mixture in

(18) Abragam, A. *The Principles of Nuclear Magnetism*; Clarendon Press: Oxford, 1961; Chapter V.

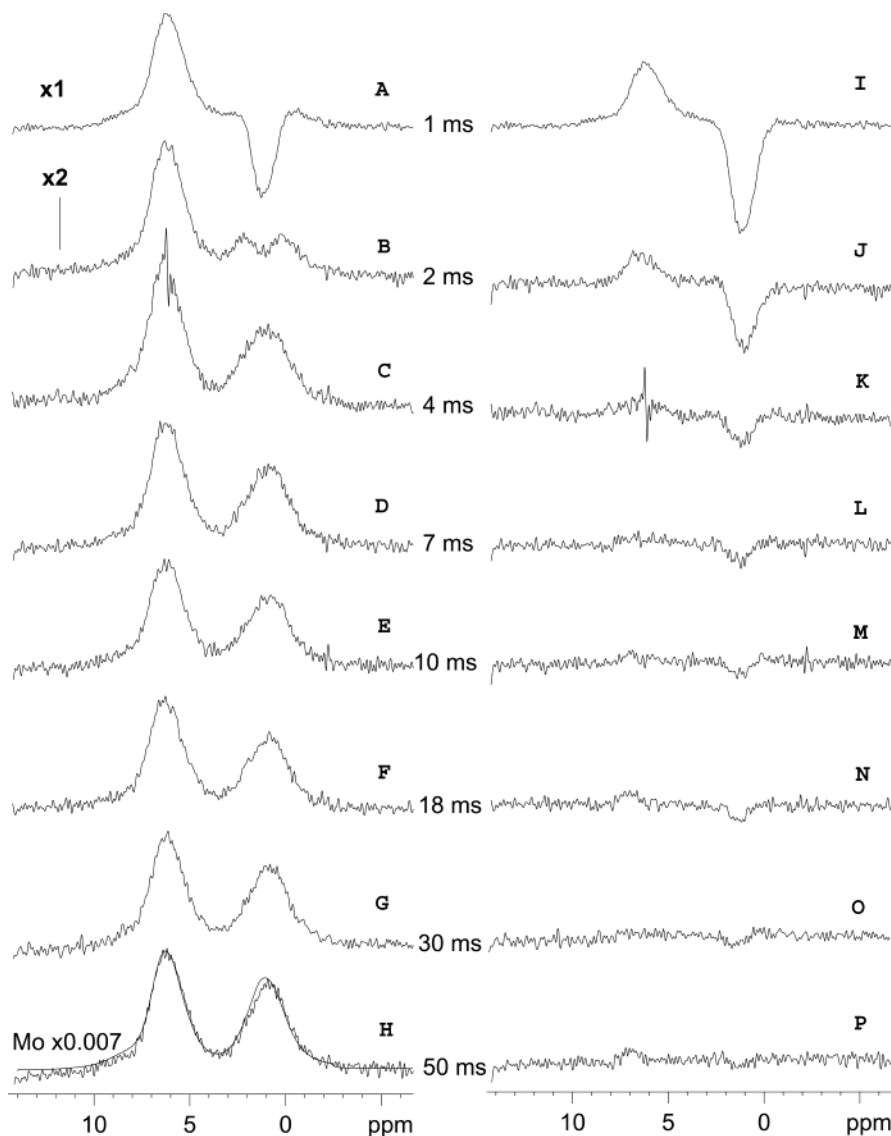


Figure 3. Spectra A–H are spin-diffusion spectra, corrected for probe background signals, at the t_{sd} values following the preparation shown in Figure 2E. Included in spectrum H is the equilibrium MREV-8 spectrum of the 91/9 blend, scaled by the factor 0.0072. Note that the spin-diffusion and the M_0 spectrum have line shapes that are very similar, indicating that internal equilibration of polarization has nearly been achieved. Note also that the narrower, negative aliphatic component near 1 ppm (from PFOS protons) is only identifiable at $t_{sd} = 1$ and 2 ms, indicating a rapid polarization exchange between the PFOS and PHS polarizations. Spectra I–P are corresponding, zero-integral difference spectra (see text for details). These latter spectra represent equal and offsetting contributions from a positive PHS spectrum and a negative PFOS spectrum; moreover, amplitudes are directly related to deviations from sample-wide polarization equilibrium.

Figure 5, one can easily identify the “doublet” signatures of the crystalline PFOS as negative signals that contrast with the positive PHS signals. Spectral changes from 2 to 50 ms only reflect intensity changes traceable to T_1^H decays. In the 91/9 PS/PFOS spectrum of Figure 6, one does not readily identify the doublet PFOS signature; there is only a hint of this in the aromatic region. Presumably, dispersal in the PS matrix via solution casting creates some broadening of the PFOS spectrum. This is not surprising in view of the fact that PS is a material that can possess anisotropic magnetic susceptibility; the latter can create broadening.¹⁹ In this case, the broadening is not a guarantee that PFOS is non-crystalline. In fact, the SD difference spectra of Figure 6 show that again, in the 2 ms to 50 ms range, very

little SD occurs. This is expected for a phase-separated, thermodynamically incompatible blend.

Figure 7 is a SD plot for three phase-separated blends (i.e., the physically mixed 91/9 PHS/PFOS and the THF-cast 96/4 and 91/9 PS/PFOS blends). Also included in Figure 7 are data for the acetone-cast 55/45 PHS/PFOS blend. The latter is representative of all of the four acetone-cast PHS/PFOS blends as can be seen from Table 1, which shows $\Delta M(t_{sd})$ values as a function of t_{sd} for all of the acetone-cast PHS/PFOS blends.

The most apparent result in Figure 7 is the rapid equilibration of the protons in the 55/45 PHS/PFOS blend compared to all of the other blends. Because of spectral overlap of the blend components, one cannot reliably obtain the average polarization for each component until intramolecular spin equilibration is nearly complete (≈ 1 ms for PHS and ≈ 2 ms for PFOS). In fact,

(19) VanderHart, D. L.; Earl, W. L.; Garroway, A. N. *J. Magn. Reson.* **1981**, *44*, 1801–1821.

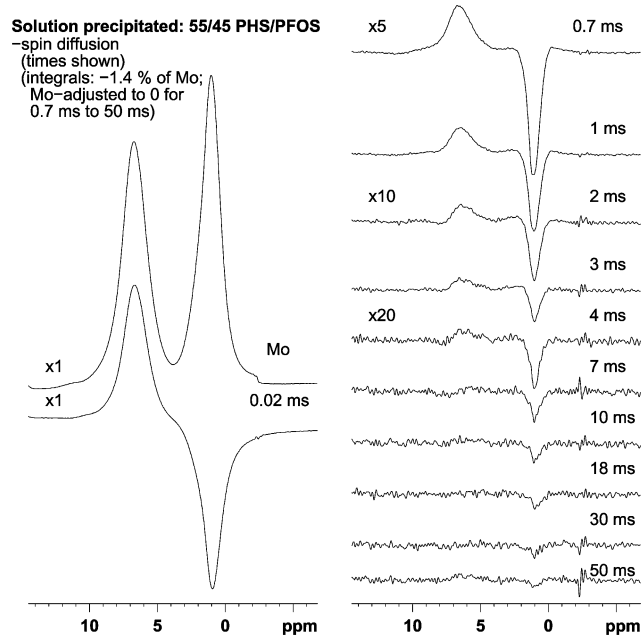


Figure 4. M_0 and zero-integral spin-diffusion difference spectra similar to those of Figure 3I–P for the acetone-cast 45/55 PHS/PFOS blend. Scaling factors are shown as are t_{sd} values. Near nulling of the spectra for $t_{sd} \geq 10$ ms indicates intimate mixing.

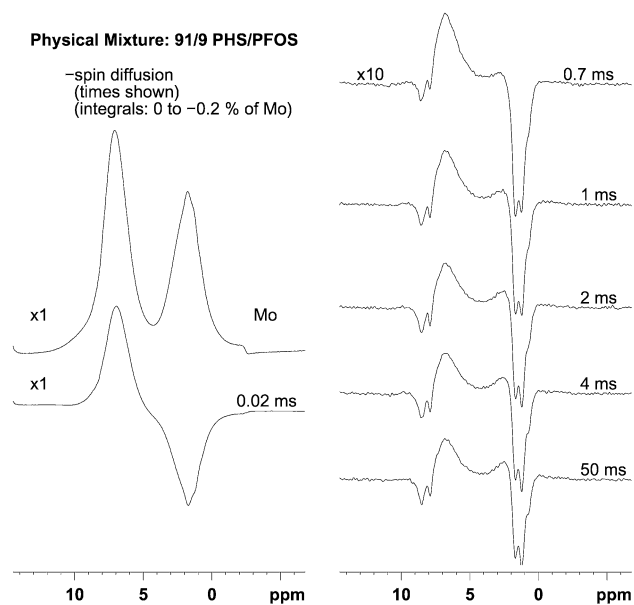


Figure 5. Spectra, including spin-diffusion difference spectra, as in Figure 4, of a 91/9 physical mixture of PHS/PFOS. Stability of line shape for $t_{sd} \geq 2$ ms shows lack of spin-diffusion coupling; splitting of negative PFOS resonances indicates PFOS crystallinity.

the $\Delta M(t_{sd})$ values of Figure 7 are based on an analysis of the aliphatic intensities alone since one can utilize two features of the PFOS aliphatic proton line shape. First, this region is more intense compared to the PFOS aromatic region; second, there is a greater ability to distinguish the PFOS and PHS resonances in this region. At $t_{sd} = 2$ ms, $\Delta M(t_{sd})$ has decayed to about 0.13, and there is no possibility of capturing an initial slope that could be used in determining a domain size. At the same time, it is clear that polarization is being exchanged between the protons of PFOS and PHS on a

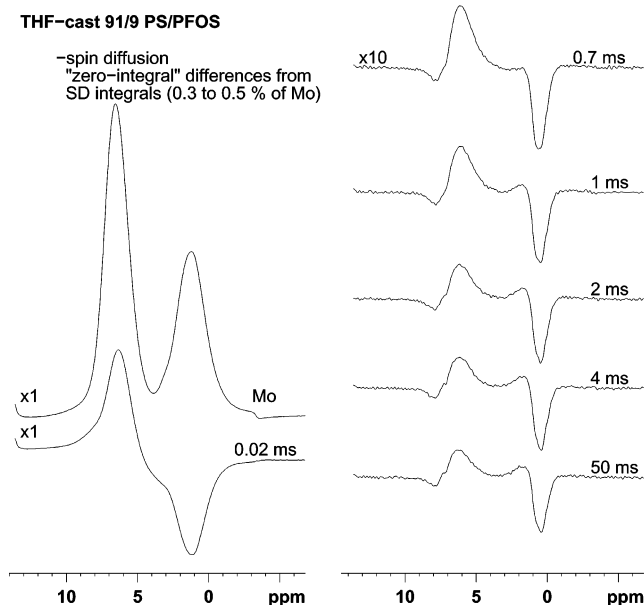


Figure 6. Spectra, including spin-diffusion difference spectra, as in Figure 4, of a THF-cast 91/9 poly(styrene)/PFOS blend. Again, stability of line shape for $t_{sd} \geq 2$ ms indicates phase separation into large domains. Splitting of negative PFOS resonances, barely visible in the aromatic region, suggests the likely existence of crystalline PFOS (see text).

similar time scale to aromatic/aliphatic polarization exchange within PFOS and within PHS. Thus, from a very qualitative standpoint, mixing in this blend, as in all of the acetone-cast blends, looks very intimate.

In contrast the other three sets of data in Figure 7 show either negligible decay (91/9 PHS/PFOS physical mixture and 91/9 PS/PFOS) or a shallow slope onward from $t_{sd} = 10$ ms. A negligible slope is indicative of very large domains and no SD between domains. For the 96/4 PS/PFOS blend, the small slope that exists would be consistent¹⁵ with spherical domains whose diameters are in the range from 0.1 to 0.2 μm , if we assume that the diffusion constants for both PFOS and PHS are equal to $0.6 \text{ nm}^2/\text{ms}$.²⁰ As discussed in the Experimental Section, scaling constants have been chosen for all of these plots, based on PFOS calibrations and assumed stoichiometries. If the scaling constants were properly determined, the intercept of each initial slope with the ordinate axis defines a $\Delta M(t_{sd})$ that relates to phase stoichiometry.¹⁵ It is a nonphysical result that such intercepts should lie above $\Delta M(t_{sd}) = 1.0$ as is seen for the PHS/PFOS physical mixture whose intercept is about 1.1. To the extent that intercepts are less than 1.0, true for the two PS blends, some component mixing is implied. A brief discussion of the intercepts in Figure 7 is included in the next section.

Discussion

Our primary interest is the characterization of the acetone-cast PHS/PFOS blends. The fact that reliable data cannot be obtained before $t_{sd} = 2$ ms means that no initial slope can be determined. Normally, this slope is the easiest way to determine domain size. At the same time, the qualitative recognition that a substantial

(20) Clauss, J.; Schmidt-Rohr, K.; Spiess, H. W. *Acta Polym.* **1993**, *1*, 44.

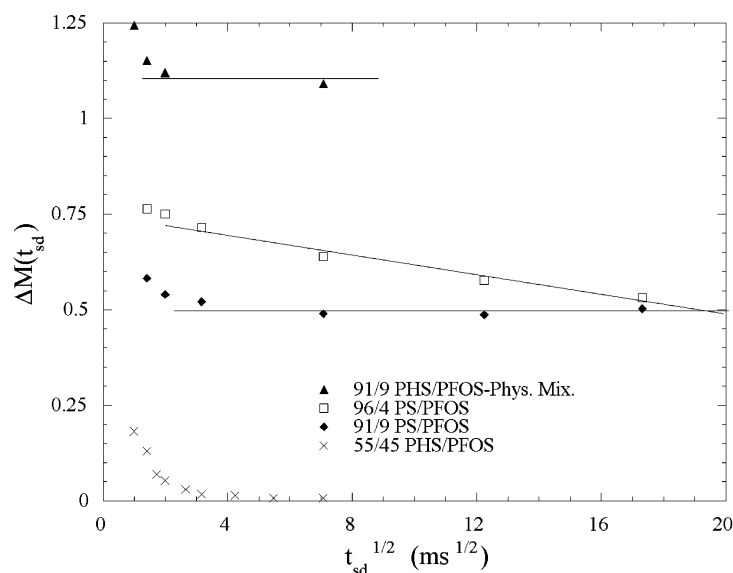


Figure 7. Spin-diffusion plots of the scaled departure of PFOS magnetization from internal spin equilibrium ($\Delta M(t_{sd})$) as defined in eq 1) vs $(t_{sd})^{1/2}$. Data correspond to the indicated blends. Only the 45/55 PHS/PFOS blend is well-mixed. The slope indicated for the THF-cast 96/4 PS/PFOS blend is suggestive of PFOS domain sizes in the 0.1–0.2 mm range while the domain size for the THF-cast 91/9 PS/PFOS blend is >0.5 mm.

Table 1. Scaled Departure from Spin Equilibrium for PFOS Proton Magnetization in a Spin-Diffusion Experiment for Acetone-Cast PHS/PFOS Blends Having the Indicated Mass Fractions^a

t_{sd} (ms)	$\Delta M(t_{sd})^b$			
	(91/9)	(85/15)	(70/30)	(55/45)
2	0.16 ± 0.03	0.11 ± 0.03	0.070 ± 0.020	0.140 ± 0.015
4	0.06 ± 0.02	0.04 ± 0.01	0.025 ± 0.020	0.053 ± 0.013
7	0.03 ± 0.01	0.03 ± 0.01	0.015 ± 0.020	0.030 ± 0.010
10	0.02 ± 0.01	0.02 ± 0.01	0.015 ± 0.007	0.017 ± 0.008
18	0.02 ± 0.01	0.02 ± 0.01	0.015 ± 0.007	0.014 ± 0.007
30	0.01 ± 0.01	0.01 ± 0.01	0.015 ± 0.007	0.007 ± 0.005
50	0.01 ± 0.01	0.01 ± 0.01	0.015 ± 0.007	0.007 ± 0.005

^a Data are based on spectra like those shown in Figures 3 and 4, and $\Delta M(t_{sd})$ is defined in eq 1. ^b Uncertainties are estimated standard uncertainties, based on 2 standard deviations, which do not include those uncertainties arising from the assumptions about the existence of intramolecular spin equilibrium outlined in the text.

amount of intermolecular SD has occurred during the 2 ms required for intramolecular spin equilibration implies that intermolecular proton–proton distances and SD pathways are not much different from intramolecular distances and pathways.

Acetone-Cast PHS/PFOS Blends. Compared to the expected linearity of the initial slope, the longer-time decay over the approximate range $0.20 > \Delta M(t_{sd}) > 0.0$ is usually very nonlinear, with the rate of decay depending on a variety of things, including the stoichiometry of the sample and the dimensionality of the diffusion problem. A conservative argument for establishing an upper limit for the domain size of the PFOS in, say, the 55/45 PHS/PFOS blend, is to compare the observed decay with the published²¹ $\Delta M(t_{sd})$ values for the spin equilibration of the aromatic and aliphatic protons of pure PS. This is truly a three-dimensional diffusion problem, just as one would expect the 55/45 PHS/PFOS problem to be. Given that the distance between protons across an aromatic ring is 0.5 nm, we

will use 0.5 nm as a characteristic aromatic or aliphatic “domain size” in PS. Comparison of the t_{sd} values, at a given $\Delta M(t_{sd})$, for PS and for the 55/45 blend, show t_{sd} values shorter by a factor of about 4 for PS when $\Delta M(t_{sd}) = 0.18$; this factor grows to about 11 for $\Delta M(t_{sd}) = 0.13$ and to about 20 for $\Delta M(t_{sd}) = 0.015$. In other words, $\Delta M(t_{sd})$ tails off, in a relative sense, more slowly for intermolecular SD in the blend than for intramolecular SD in pure PS. One reason for this is that expected concentration fluctuations can have an influence on the approach to final equilibrium for a blend, whereas corresponding aliphatic/aromatic fluctuations are absent in the monomer structures of PS. Given that the square root of time and distance are generally proportional in diffusion problems, even the larger factor of 20 in the above comparison would translate into a domain size of only 2.3 nm [= (0.5 nm)(20)^{1/2}] for PFOS in the 55/45 PHS/PFOS blend. Thus, we view this 2.3 nm estimate to be an upper limit on the domain size of the PFOS. Certainly, the implicit assumption in this latter comparison (i.e., that the diffusion constant of PS is appropriate to PHS and PFOS) is conservative. We do not expect the latter diffusion constants to be larger, owing to the dilutions of proton density with oxygen atoms for PHS and with sizable perfluorinated entities for PFOS. Also, the fact that the ratio of t_{sd} values for a given $\Delta M(t_{sd})$ grows as $\Delta M(t_{sd})$ goes to zero probably means that if we could see the initial slopes, they would probably differ by less than a factor of 2, implying that the average PFOS domain size is likely to be closer to 1 nm.

In our minds, it is not critical to be precise in determining the PFOS domain size of these acetone-cast blends. For our purposes, it is sufficient to show that the mixing is intimate (i.e., on a scale of a few molecular diameters). Given that that this structure develops as the acetone leaves and that PFOS has very modest molecular mass, one would not expect the kinetics of glass formation to be so rapid as to produce

(21) VanderHart, D. L. *Macromolecules* **1994**, *27*, 2837–2845.

such an intimate mixture of PHS and PFOS unless there were thermodynamic compatibility between these components. Hence, we are claiming that on the basis of the NMR measurements PHS and PFOS are thermodynamically compatible.

By way of completeness, it is commonly found in our SD data for well-mixed blends that $\Delta M(t_{sd})$ does not exactly go to zero at longer t_{sd} as is indicated in Table 1. Asymptotes are typically in the range of 0.01 with some comparable uncertainty. Whether this is an experimental artifact or whether it is real can be debated. However, if it were real, it would indicate that not all regions have the same composition. Such nonzero asymptotes create larger ambiguities in composition for samples which have smaller amounts of PFOS. Without going into a lot of detail, the asymptote is much more sensitive to the possibility that a fraction of the minor component (PFOS) remains unmixed than to the possibility that a fraction of the major component (PHS) remains unmixed. Thus, from the asymptotes given in Table 1, we can conclude that at least 97.8% of the PFOS is mixed with PHS. On the other hand, it is not so clear that, for example, all PHS domains are mixed (i.e., pure PHS domains could exist). In fact, for the 91/9 acetone-cast blend, as much as 35% of the PHS could exist as a pure domain and one could still rationalize an asymptote of 0.02. In contrast, for the 55/45 sample with the highest PFOS composition (asymptote ≤ 0.012) only 4.5% of the PHS could exist as a pure PHS phase and still preserve the asymptote. Even with the ambiguities in composition that are associated with the blend data of Table 1, there is no binary phase diagram that can be drawn for PFOS and PHS where phase separation at ambient temperature is predicted and where the composition of the PHS-rich phase can be held appropriately constant for all blends in keeping with the data. Hence, if these blends represent the equilibrium state at ambient temperature, then they are fully compatible and the nonzero asymptote is mainly an experimental artifact.

Given the foregoing discussion, if heterogeneity of composition exists on a large scale, say, greater than 50 nm, there is a simple experiment that might show such heterogeneity. It involves taking a "zero-crossing" spectrum in an inversion recovery experiment with CRAMPS readout. Since the components have intrinsically different T_1^H values (765 ms for pure PFOS and 1.22 s for PHS), and if there are different phases with different compositions, then following inversion of the magnetization and a suitable delay time, one can capture the signal near its null-integral condition. This zero-crossing signal would then be the sum of a positive contribution from one phase and an offsetting negative contribution from the other domain. The different chemical compositions of the domains would translate into a line shape that could be recognized as having, in this case, contributions of opposite sign from PFOS and PHS. Figure 8 shows the CRAMPS spectrum of the 91/9 physical mixture (Figure 8A) and the 91/9 blend (Figure 8C) in the vicinity of the zero-crossing. This spectrum is also compared to an M_0 CRAMPS spectrum (Figure 8B), scaled down by a factor of 0.002. It is obvious that the physical mixture exhibits strong component separation owing to the positive PFOS signals coexisting with

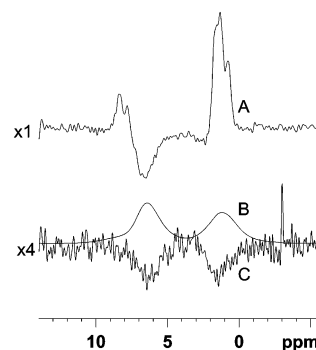


Figure 8. Two background-corrected, MREV-8, inversion-recovery spectra of 91/9 blends of PHS/PFOS taken near their "zero-crossing". Spectra illustrate the different responses when blends are phase separated into large domains (A, physical mixture) vs intimately mixed (C, acetone-cast). The positive M_0 spectrum B of the acetone-cast blend, scaled by 0.002, is also shown. Similarity of line shapes B and C indicates that the PFOS and PHS protons have identical T_1^H values in that blend; positive PFOS and negative PHS resonances in A indicate large, phase-separated domains.

the negative PHS signals at a relatively low vertical gain. In contrast, within the signal-to-noise ratio for the blend, there is no clear departure from the M_0 line shape, even for such a small signal (i.e., all components seem to have a uniform polarization). Hence, there is no indication of any large-scale phase separation. Very similar results were obtained for all four acetone-cast PHS/PFOS blends. Unfortunately, the asymmetric sensitivity of this zero-crossing experiment to the existence of pure PHS domains as opposed to pure PFOS domains is similar to that discussed for the SD data; hence, this experiment does not decisively address the possibility that a fraction of the PHS exists as a pure phase. In that sense the main effect in including Figure 8 is to confirm, qualitatively, the results of the SD experiment.

Intercepts for Phase-Separated Blends. It was noted in the previous section that the intercepts of Figure 7 for the phase-separated blends were not 1.0, as expected when phases are separated into their pure components. From the initial slopes drawn in Figure 7, there is no question that phase separation exists in view of the weak to nonexistent initial slopes. Intercepts below 1.0 can arise either because of improperly assumed overall stoichiometries or because one or both of the phases are mixed (i.e., not pure component). Intercepts above 1.0 are nonphysical and do not indicate mixed phases; more likely such intercepts indicate an improper assumption about stoichiometry. Thus, the intercept for the 91/9 PHS/PFOS physical mixture of 1.1 probably indicates a true stoichiometry closer to 90/10. On the other hand, the intercepts of the 96/4 and the 91/9 PS/PFOS blends (respectively, about 0.75 and 0.50) could indicate some mixed phases. Only a portion of each prepared sample was used for the NMR experiment. Because phase separation occurs, a stoichiometric bias may arise during sample recovery. Also, the components could have some differential affinities for the poly(tetrafluoroethylene) surface of the evaporating dish. Hence, we only use these results to show incompatibility of PS and PFOS and are not insisting on the existence of any mixed phases. It is interesting that the intercept of the 96/4 blend is larger than that of the 91/9 blend. Normally, the larger intercept is associated with

less mixing. One would expect that if a small amount of PFOS could dissolve into a PS-rich phase, then increasing the concentration of PFOS should result in a larger fraction of the PFOS being found in the pure-PFOS phase. This would appear as poorer mixing, contrary to what is observed. On the other hand, if a small amount of PS could dissolve in the PFOS-rich phase, then an approximate doubling of the amount of PFOS should result in about the same stoichiometry for the PFOS-rich phase and about the same intercept; this is again contrary to observation. Hence, the PS/PFOS intercepts are, in our opinion, more likely to be explained by variations of stoichiometry rather than by the existence of mixed phases.

Attempt to Detect ^{19}F - ^1H Dipolar Interactions.

Although the SD data for the acetone-cast PHS/PFOS blends provide a convincing case for intimate mixing, it also seemed reasonable that such mixing would lead to detectable dipolar interactions between the protons of PHS and the ^{19}F nuclei of PFOS. PFOS contains several ^{19}F nuclei; moreover, the strength of a ^{19}F dipole is comparable to that of a proton. Internuclear distances could, in principle, get as close as 0.3 nm; there would probably be several contacts in the 0.3–0.5 nm range with associated dipolar interactions in the range of 4–0.9 kHz. An indication that there might be something wrong with this reasoning is the proton CRAMPS spectrum of the pure PFOS in Figure 2C. Despite the high density of ^{19}F nuclei in this sample, the spectrum has sharp lines. Moreover, the intensity ratio of aromatic to aliphatic resonances is exactly that expected from the chemical formula, indicating that neither the aliphatic nor the aromatic protons have important differences in the strength of their dipolar couplings to ^{19}F nuclei. Given that this experiment is conducted with only 2.5 kHz MAS and given that the MREV-8 sequence, used to obtain the CRAMPS spectrum, should only scale the ^{19}F - ^1H dipolar interactions by a factor⁸ close to 0.5, it was at first surprising that the lines were quite narrow. Moreover, in the sense that MAS should to a first approximation average away the dipolar interactions, it was also interesting that the first spinning sidebands (not shown) of the 91/9 blend and of the PHS spectra of Figure 2 were essentially identical. If the ^{19}F - ^1H dipolar broadening were competitive with the proton chemical shift anisotropy (1–2 kHz range) in interaction strength, these sidebands should have been much more intense. Therefore, in an effort to avoid MAS averaging of the ^{19}F - ^1H dipolar interactions, we took nonspinning MP spectra of PHS, PFOS, and the 91/9 PHS/PFOS blend. These are shown in Figure 9. In these spectra the apparent resolution is substantially deteriorated, relative to the spectra of Figure 2, because of the fact that chemical shift anisotropies are present as are nontrivial magnetic susceptibility effects arising from particle shapes. The spectrum of PFOS is definitely broader than that of PHS or the blend; presumably, the PFOS protons experience additional broadening from the ^{19}F - ^1H interactions. In contrast, additional broadening in the blend spectrum, relative to PHS, is hardly noticeable. One might conclude from the similarity of sideband intensities and static line shapes that PFOS is, in fact, not mixed on a molecular level in the blend. However, the counterevidence for molecular level mixing

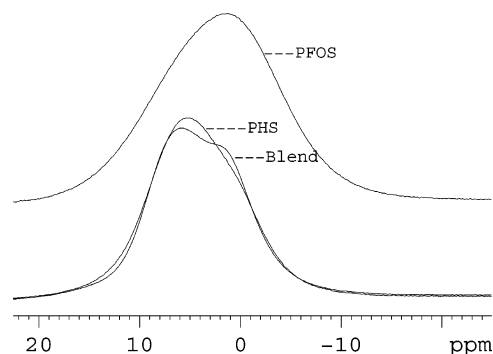


Figure 9. Nonspinning MREV-8 spectra of the indicated materials; “blend” refers to the 91/9 acetone-cast blend. We are looking for evidence of the intimate mixing of the PHS protons with ^{19}F nuclei of PFOS via a broadening from ^1H - ^{19}F dipolar coupling. This broadening is not detectable, mainly as a result of ^{19}F - ^{19}F polarization-exchange events that are rapid on the time scale of intermolecular ^1H - ^{19}F couplings. There is some additional ^1H - ^{19}F broadening associated with the pure-PFOS spectrum, owing to the high concentration of ^{19}F nuclei.

from proton SD is very strong. In our opinion, the explanation for the lack of significant ^{19}F - ^1H dipolar broadening in the blend is a combination of two effects: (a) a rather high dilution of the fluorinated portions of the PFOS and (b) strong spin exchange interactions between the 17 ^{19}F nuclei on each of the perfluorinated PFOS segments. These latter interactions cause the apparent ^{19}F Zeeman states to fluctuate on a time scale shorter than the time scale of the weaker ^{19}F - ^1H intermolecular dipolar interactions. The latter has the effect of substantially self-decoupling²² the ^{19}F and proton spins. It is most likely that, in the coupling period of any proposed experiment specifically designed to detect ^{19}F - ^1H dipolar couplings between PFOS and PHS nuclei, one would have to apply some irradiation to the ^{19}F nuclei that would suppress ^{19}F - ^{19}F spin exchange. We cannot perform such experiments with our current instrumentation.

NMR has been used previously²³ to investigate the mixing of ammonium trifluoromethanesulfonate, a PAG analogue, and PHS. In that study, phase separation of the PAG was seen at concentrations above a mass fraction of $9 \pm 2\%$ where the indicator of PAG aggregation was the development of ^{19}F multiple-quantum coherences greater than 3 (arising from more than three dipolar-coupled ^{19}F nuclei). We did not take the same approach in our case since, with 17 ^{19}F nuclei on each PAG molecule, one would have to look for multiple-quantum coherences higher than 17. This is impractical here because of the rapidly weakening signals from higher order coherences, even in the case where strong aggregation would favor the build-up of higher-order coherences.

General Remarks. ^{13}C NMR has also been used²⁴ to measure independently the rotating-frame relaxation times ($T_{1\rho}^{\text{H}}$) of the protons belonging to different photoresist components, namely, the reactive copolymer and

(22) Abragam, A.; Winter, J. C. R. *Acad. Sci.* **1959**, *249*, 1633.

(23) Limb, S. J.; Scruggs, B. E.; Gleason, K. K. *Macromolecules* **1993**, *26*, 3750–3757.

(24) Mirau, P. A.; Heffner, S. A.; Rushkin, I.; Houlihan, F. M. In *Advances in Resist Technology and Processing XVII*; Houlihan, F. M., Ed.; Proceedings of SPIE Vol. 3999; 2000; pp 104–111.

a dissolution inhibitor. Our approach offers a slightly more accurate indication of the level of mixing; however, all of the above methods, including our own, have some difficulty in differentiating a situation of uniform mixing of a very minor species throughout the entire polymer versus a good dispersion of the minor species in only a portion of the polymer.

It was found in a process-optimization experiment by Petrillo et al.²⁵ using related photoresists that PAG concentration was an important variable in determining the quality of the final nanostructure. In that work variables also included post-apply-baking and post-exposure-baking times and temperatures. While the conclusions reached did not directly address the issues of PAG miscibility, it was concluded that, for certain systems, a decrease in PAG concentration leads to improvements in feature resolution. Heterogeneous distributions of PAG at the higher concentrations may be at the origin of this behavior, consistent with the notion that thermodynamic compatibility is an important equilibrium property. Aggregation or phase separation of PAG within the photoresist might limit the diffusive length of PAG within a given post-exposure-baking time and that could lead to observed faults in the final developed structure, such as line edge roughness.

Thermodynamic compatibility in bulk samples, while presumed necessary for good PAG distribution, does not absolutely ensure uniformity of concentration in thinner films (ca. 0.1 μm) typical of photoresists. Component distribution can also be influenced by the relative attractions of the components for the air/blend and substrate/blend interfaces. For example, in one recent study²⁶ using techniques of Rutherford Backscattering Spectrometry (RBS) and Secondary Ion Mass Spectroscopy (SIMS), a PAG (analogous to PFOS but substituting the triflate anion) was observed to show a degree of concentration enhancement at the substrate interface based on the degree of hydrophilicity of the substrate surface. In another study, RBS was used to probe the miscibility between several different PAG and photoresist systems.²⁷ In a very recent study,²⁸ near edge X-ray absorption fine structure (NEXAFS) was employed in the study of 95/5 PHS/PFOS films (about 100 nm thick, cast from low-volatility propylene glycol methyl ether acetate). Those authors reported a significant enhancement of PFOS concentration in the first 3–5 nm of depth from the air/polymer interface after a sub- T_g post-apply baking. After UV exposure, they observed that more of the fluorinated component of the exposed PFOS was drawn away into the interior of the film. This trend continued upon post-exposure baking above the T_g of PHS. Note that the inherent in-plane compositional averaging with NEXAFS, RBS and SIMS

techniques foregoes any in-plane nanometer-length-scale interpretation; thus, the NMR investigations in the present study can also be used to complement these routine thin-film experiments.

The possible segregation of PAGs, such as PFOS, to air/blend and substrate/blend interfaces will always be an issue that is more properly addressed by experimental techniques such as RBS and NEXAFS. PAG-containing photoresist films might also show some level of PAG segregation as a result of other considerations including differential solubilities in a slowly evaporating casting solvent with ensuing kinetic entrapment of concentration gradients or phase separation induced by thermal cycling. However, for any polymer/PAG blend, thermodynamic compatibility in the bulk is an important property to demonstrate if one hopes to minimize concentration gradients.

Conclusions

Using multiple-pulse proton SD techniques, we have been able to determine that for bulk samples the photoacid generator di(*tert*-butylphenyl)iodonium PFOS used in photolithography, when present at mass fractions from 9% to 45%, is intimately mixed with the amorphous PHS matrix such that domains of PFOS, in minimum dimension, are near molecular dimensions (i.e., less than 2.3 nm and probably closer to 1 nm). Moreover, given very low-level uncertainties in the asymptotic data at longer t_{sd} , some regions of heterogeneous composition could exist. While it is clear that at least 97.8% of the PFOS is dispersed into the PHS, in principle up to 35% (91/9 blend) or 4.5% (55/45 blend) of the PHS could be phase separated as an unmixed phase and still be consistent with the data. However, it is judged that the small, nonzero, asymptotic values are controlled by experimental artifacts rather than compositional heterogeneity. It is also argued that PHS and PFOS are thermodynamically miscible because kinetic entrapment into domains as small as 2.3 nm would not occur under the preparation conditions if PHS and PFOS were incompatible. Hence, given this miscibility, we deduce that in bulk samples, below a mass fraction of 0.45, the PFOS should be uniformly distributed in the PHS. For thin films therefore any heterogeneity of concentration of these components would most likely arise from alternate considerations (e.g. preferential interface affinity or differential solubility in the casting solvent).

As a contrast to the miscible PHS/PFOS blends, we also looked at a physically mixed, 91/9 blend of PHS/PFOS to demonstrate data taken in the absence of measurable SD. We also included two THF-cast samples of poly(styrene)/PFOS blends (96/4 and 91/9). Time dependence of the data unambiguously indicated phase separation into PFOS domains exceeding 0.1 μm in these materials. However, intercepts for the latter data were not exactly those expected for phase separation into pure-component phases. This situation could be explained by either partially mixed phases or uncertainty in the overall stoichiometry of the blends. Since, for a phase separated system, the overall stoichiometry of the sample is not necessarily preserved when taking a portion for the NMR experiment, no claims are being made that any mixed phase exists in the PS/PFOS system.

(25) Petrillo, K. E.; Pomerene, A. T. S.; Babich, E. D.; Seeger, D. E.; Hofer, D.; Breyta, G.; Ito, H., *J. Vac. Sci. Technol. B* **1994**, *12*, 3863–3867.

(26) Lin, Q.; Angelopoulos, M.; Babich, K.; Medeiros, D.; Keimel, C.; Sundararajan, N.; Weibel, G.; Ober, C. *Forefront of Lithographic Materials Research*; Society of Plastics Engineers: Brookfield, CT, 2001; p 347.

(27) Uhrich, K. E.; Reichmanis, E.; Baiocchi, F. A. *Chem. Mater.* **1994**, *6*, 295–301.

(28) Lenhart, J. L.; Jones, R. L.; Lin, E. K.; Soles, C. L.; Wu, W.-li, Fischer, D. A.; Sambasivan, S.; Goldfarb, D. L.; Angelopoulos, M. J. *Vac. Sci. Technol.* **2002**, *B20*, 2920–2926.

We emphasize that the observation of phase separation into rather large domains for the PS/PFOS blends is not necessarily proof of thermodynamic incompatibility. While such incompatibility is suspected, there is also the possibility that strongly differential solubility in THF for PFOS and PS could explain the observed segregation. In that sense, the observation of intimate mixing for PHS/PFOS blends is a more definitive result because thermodynamic compatibility is the only conclusion.

The SD methods that we have utilized can be generally applied to the study of component mixing so long as there are spectral distinctions, in the equilibrium spectra, that are adequate for evaluating the signals from each component. These spectral distinctions do not necessarily require a spectral region where only one component appears, as was illustrated in the current work where spectral overlap was strong, yet intensity distributions were sufficiently different. It is also easier

to apply this technique when neither of the components has a high mobility (i.e., when proton–proton dipolar couplings are strong so that good estimates of the spin-diffusion constants can be made). We are currently making similar measurements on blends of PFOS and copolymers that are more typical of those used in photolithography. We are also investigating some of the candidate materials for 157 nm lithography.

Acknowledgment. This work was carried out, in part, under a Defense Advanced Research Projects Agency contract (N66001-00-C-8083) and is an official contribution of the National Institute of Standards and Technology. We also thank IBM for supplying the materials. V.M.P. is grateful for support from the National Research Council/National Institute of Standards and Technology Postdoctoral Fellowship Program.

CM030130H